Author Manuscript

Author Manuscript

Author Manuscript

Author Manuscript

HHS Public Access

Author manuscript

Methods Mol Biol. Author manuscript; available in PMC 2019 June 10.

Published in final edited form as:

Methods Mol Biol. 2017 ; 1487: 337–351. doi:10.1007/978-1-4939-6424-6_25.

Reconstructing ERK Signaling in the *Drosophila* Embryo from Fixed Images

Bomyi Lim[1,2], **Carmeline J. Dsilva**[1], **Ioannis G. Kevrekidis**[1,3], and **Stanislav Y. Shvartsman**[4,5]

[1] Department of Chemical and Biological Engineering, Princeton University, Princeton, NJ, 08544, USA.

[2] Lewis-Sigler Institute for Integrative Genomics, Princeton University, Princeton, NJ, USA.

[3] Program in Applied and Computational Mathematics, Princeton University, Princeton, NJ, USA.

[4] Department of Chemical and Biological Engineering, Princeton University, Princeton, NJ, 08544, USA.

[5] Lewis-Sigler Institute for Integrative Genomics, Princeton University, Princeton, NJ, USA.

Abstract

The early *Drosophila* embryo provides unique opportunities for quantitative studies of ERK signaling. This system is characterized by simple anatomy, the ease of obtaining large numbers of staged embryos, and the availability of powerful tools for genetic manipulation of the ERK pathway. Here, we describe how these experimental advantages can be combined with recently developed microfluidic devices for high throughput imaging of ERK activation dynamics. We focus on the stage during the third hour of development, when ERK activation is essential for patterning of the future nerve cord. Our approach starts with an ensemble of fixed embryos stained with an antibody that recognizes the active, dually phosphorylated form of ERK. Each embryo in this ensemble provides a snapshot of the spatial and temporal pattern of ERK activation during development. We then quantitatively estimate the ages of fixed embryos using a model that links their morphology and developmental time. This model is learned based on live imaging of cellularization and gastrulation, two highly stereotyped morphogenetic processes at this stage of embryogenesis. Applying this approach, we can characterize ERK signaling at high spatial and temporal resolution. Our methodology can be readily extended to studies of ERK regulation and function in multiple mutant backgrounds, providing a versatile assay for quantitative studies of developmental ERK signaling.

Keywords

ERK dynamics; Quantitative imaging; *Drosophila* embryo

stas@princeton.edu.

Author Manuscript Author Manuscript Author Manuscript Author Manuscript

1 Introduction

The extracellular signal regulated kinase (ERK) plays a key role in a wide range of developmental contexts and must be tightly regulated in both space and time [1]. Indeed, mutations and chromosomal deletions that lead to either reduced or increased levels of ERK activation can result in developmental abnormalities, such as facial dysmorphisms and congenital heart defects observed in humans with gain-of-function mutations in ERK pathway components [2, 3]. Mechanistic understanding of these defects makes it important to analyze developmental functions of ERK quantitatively, beyond establishing its necessity in a given process.Quantitative parameters of ERK activation in developing tissues remain poorly understood, largely because of the lack of highresolution information about ERK signaling as a function of space, time, and genetic background.

Recently, we have used a combination of imaging and computational approaches to provide a high-resolution picture describing ERK activation and signaling in the early *Drosophila* embryo, an experimental system that lends itself to quantitative studies [4, 5]. Here, we illustrate our approach by describing a sequence of steps leading to the temporal reconstruction of a pulse of ERK activation, which is necessary for patterning the future nervous system. This reconstruction protocol is particularly useful because no methods are yet available to monitor ERK activation in live embryos.

ERK is activated when it is doubly phosphorylated, and its activity can be detected using an antibody that recognizes the dually phosphorylated form of ERK (dpERK) [6]. In early fly embryos, ERK is activated first at the poles of the embryo to give rise to terminal structures,~1.5–2 h after egg-laying, from nuclear cycle (NC) 11 to 14. ERK activity disappears from the poles during mid-NC 14 (~2.5 h after egg-laying), and it is activated again in both sides of the embryo, distributed in two longitudinal stripes that span 10–13 cells along the dorsoventral (DV) axis. In both processes, ERK activation leads to transcriptional induction of specific genes: *huckebein (hkb)* at the poles and *intermediate neuroblasts defective (ind)* at the lateral ectoderm [7, 8].

We developed a systematic approach for reconstructing the phase of ERK activation leading to *ind* expression during the third and fourth hours of embryonic development (Fig. 1a). Our dynamics reconstruction is based on the quantitative matching of fixed embryo morphologies to morphogenetic events recorded from live embryos (Fig. 1c). Initially, the embryo is a syncytium where nuclei are arranged in a monolayer under the common plasma membrane. After 13 mitotic divisions, the embryo undergoes cellularization and the monolayer of nuclei is transformed into an epithelial sheet, forming a cellular blastoderm. The embryo then undergoes gastrulation, ~3 h after egg-laying. Morphological changes during the cellularization and gastrulation processes can be characterized as a function of time. By associating shape changes with time, we can use the morphological features of any fixed embryo to estimate its developmental age. Below we describe the data collection and analysis steps needed to reconstruct the ERK-dependent induction of *ind.*

Author Manuscript Author Manuscript Author Manuscript Author Manuscript

2 Materials

2.1 Embryo Preparation and Staining

1. Embryo collection: embryo collection cages, apple juice plates, and yeast paste.
2. Dechorionation: mesh, 50 % bleach (2.5 % sodium hypochlorite solution), and distilled water.
3. Phosphate-buffered saline (PBS).
4. Fixation and devitellinization: we use 4 % formaldehyde (37 % stock solution) in PBS as fixative. This solution is saturated with an equal volume of heptane in scintillation vials. Devitellinization is carried out using a methanol:heptane (1:1) mixture.
5. Primary antibodies: anti-dpERK and other primary antibodies (specific antibodies used in Figs. 1 and 7 are described in the corresponding figure legends).
6. Secondary antibodies: species-specific antibodies conjugated to Alexa Fluor® dyes or other fluorochromes.

2.2 Embryo Loading and Imaging

1. Microfluidic device setup: Microfluidic Embryo Trap Array, pressure source (O_2), pressure gauge, inlet and outlet reservoir, tubing, and stereo microscope.
2. PBST: 0.02 % Triton-X 100 in PBS.
3. 90 % glycerol.
4. Confocal microscope with up to four lasers and brightfield light and ×60 oil immersion objective.
5. Halocarbon Oil 27.

2.3 Developmental Timing of Fixed Embryos

1. MATLAB® (Release 2013b, The MathWorks, Natick, Massachusetts) and ImageJ [9] software packages are used for image processing and time estimation analysis.

3 Methods

The general outline of our reconstruction method is as follows: we first take live time-lapse movies of the cellularization and gastrulation processes and use these data to build a function from morphological features to developmental time. In parallel, fixed embryos are stained with protein antibodies or mRNA probes of interest, as well as with markers that visualize relevant morphological features (e.g. membrane-bound proteins or nuclei markers). In both live and fixed imaging, we use the microfluidics platform to take DV cross-sectional images of embryos (Fig. 1b). Imaging is done using confocal microscopes, and the images are converted to TIFF files using ImageJ. The developmental time of each fixed embryo is

Author Manuscript Author Manuscript Author Manuscript Author Manuscript

estimated using a function constructed from the live imaging data. Then, the protein and gene expression dynamics are reconstructed by ordering the embryo snapshots in time and extracting signals from a cell or region of interest.

3.1 Imaging Live and Fixed Samples in the Microfluidic Device

To analyze ERK signaling during nuclear cycle 14, we collect embryos for 3 h (*see* Note 1). Typically, apple plates are placed under an embryo collection cage with ~100–200 flies. Chorions of both live and fixed embryos are removed by soaking embryos with 50 % bleach for ~1 min. After dechorionation, live embryos are ready to be loaded into the microfluidic device for end-on imaging. For fixed samples, conventional immunostaining and fluorescence in situ hybridization (FISH) protocols are followed after dechorionation, and embryos are loaded after the completion of staining procedures (*see* Note 2) [10, 11].

To visualize the embryos, a Microfluidic Embryo Trap Array is prepared (Fig. 1b). A detailed protocol for the fabrication of the device is available in Levario et al. [12]. Steps of embryo loading into the microfluidic device are similar for both live and fixed samples. An empty device is connected with inlet and outlet reservoirs, and the pressure is increased to ~10–15 psi. The loading fluid (PBS) will flow into the device upon pressure increase. During the initial fluid-filling process, it is essential to remove all air bubbles trapped in the device, since they can prevent embryos from flowing into the chambers (*see* Note 3). When the entire chambers and channels are filled with PBS, pressure is decreased to ambient conditions.

Embryos are then inserted into the inlet reservoir, with ~50 mL of PBST or PBS, for live and fixed embryos, respectively; PBST is used to load live embryos since they will stick to the tubing in PBS buffer. The inlet reservoir is wrapped with Parafilm® to provide an airtight seal. For embryo loading, pressure is increased to ~10 psi (*see* Note 4). During loading, we gently tap the bottom of the device (not directly on the channel, but below) with a pen to help the transfer of embryos into the chambers. Tapping also helps clear up embryos trapped in the channel. The inlet reservoir is swirled from time to time to facilitate the embryo flow. Once enough embryos are loaded onto the device, pressure is decreased back to ambient level.

For fixed embryos, PBS is replaced with 90 % glycerol to match the refractive index of the objective used in the microscope, while we keep PBST for live embryos (*see* Note 5). After loading, the device is disconnected from the inlet and outlet reservoirs. We seal the inlet and

---

1. For live imaging, we usually employ *Drosophila* transgenic lines that express a particular fluorescently tagged protein that can be tracked in vivo (*see* Subheading 3.2).
2. Any proteins or mRNAs of interest can be analyzed, but it is essential to costain a protein that is ventrally localized (i.e. Dorsal or Twist) for upright imaging. Embryos need to be aligned so that the ventral side can be located at the bottom of a captured image.
3. Gentle tapping on the device with a pen will help remove the air bubbles trapped in the channels. Some bubbles can also be removed by increasing the pressure to ~15–20 psi with both inlet and outlet valves closed and waiting about 10 min.
4. While our average pressure for loading is ~10 psi, this can be adjusted from 7 to 15 psi as needed. Note that higher pressure increases the chance of embryos being squeezed.
5. For typical live imaging, halocarbon oil is used, as it allows oxygen diffusion and has a refractive index similar to that of glycerol. However, halocarbon oil damages the microfluidic device such that it is not recyclable. Instead, we typically use PBST for loading embryos into the device. A drawback of using PBST is that it can degrade image resolution, since PBST has a refractive index lower than that of glycerol. If high-resolution imaging is necessary, PBST can be replaced with halocarbon oil and the device will need to be discarded afterwards.

Author Manuscript Author Manuscript Author Manuscript Author Manuscript

outlet holes with tape, and the loaded device is taken to a microscope for imaging. Within the device, all embryos are oriented in “end-on” position, with either their anterior or posterior pole facing towards the coverslip. This facilitates DV cross-section imaging. Once mounted in the microscope, we can move the device to visualize different embryos along the microfluidic channel.

For live imaging, we typically pick embryos in NC 13 to capture the entire cellularization and gastrulation processes (*see* Note 6). For fixed imaging, we capture all the embryos that are in NC 14. For both live and fixed imaging, we capture images on a plane across the DV axis of an embryo, at the same anteroposterior (AP) location along the embryo (Fig. 1c). In general, images are taken ~90 μm away from the posterior pole, to reduce variations resulting from morphological differences between the anterior and posterior regions.

Once imaging is completed, the device can be cleaned by flowing distilled water or PBS in reverse direction, from outlet to inlet. This will force embryos out of the chambers so that the device can be reused.

3.2 Estimating the Developmental Times of Images During Cellularization

Developmental time estimation via morphological matching is straightforward during cellularization, where we can use the lengths of lateral membranes as a proxy for time. In this process, nuclei that are located under the common plasma membrane are enclosed by lateral membranes which grow gradually inward, separating the nuclei into individual cells [13]. The lengths of lateral membranes monotonically increase with time with highly reproducible kinetics [14].

The cellularization process can be monitored via live imaging, either using brightfield optics, or through fluorescence microscopy using transgenic lines that express membrane-bound molecules tagged with fluorescent proteins such as GFP. A convenient marker for the cellularization process is the myosin regulatory light chain Spaghetti squash fused to GFP (Fig. 2a). During the first 40 min of nuclear cycle 14, the cell membrane slowly invaginates between the nuclei, and these begin to elongate. During the subsequent 20 min, the membrane furrows invaginate further inward with increasing speed, until they close at the basal ends of nuclei. At the end of cellularization, each cell is approximately 35 μm long. The calibration curve that relates membrane ingression length to developmental time can be generated using six time-lapse movies of Sqh-GFP embryos (Fig. 3a) (*see* Note 7). The error can be calculated as the standard error of the mean of six movies.

Using this calibration curve, we can estimate the developmental age of each fixed embryo by measuring the length of its membrane furrows. We can measure this length either by taking phase-contrast images, or by costaining embryos with a membrane marker (Fig. 3b). It is also possible to verify that membranes visualized under phase-contrast colocalize with the fluorescent signals of membrane markers. With this method, the developmental age of fixed embryos undergoing cellularization can be estimated with an accuracy of 1–2 min.

6. Live imaging should be conducted at constant temperature, as the rate of development is temperature-dependent.
7. When multiple live imaging experiments are used, $t = 0$ must be chosen consistently between experiments. For our analyses, we select $t = 0$ immediately following the 13th mitosis, but it could also be chosen based on a specific morphological event.

Author Manuscript Author Manuscript Author Manuscript Author Manuscript

3.3 Estimating the Developmental Times of Images During Gastrulation

In general, to estimate the stage of fixed images, we require two components: (1) the appropriate independent variables or observables which can be used to describe the dynamics, and (2) a function which uses these independent variables to map each image to time. During gastrulation, the morphology changes are complex and there is no clear single independent variable (analogous to membrane length during cellularization) which describes the developmental progress. We therefore use an approach that requires little a priori knowledge about the developmental dynamics. We found that this approach can capture the complex changes in gastrulation, and is potentially applicable to other developmental processes.

To monitor the gastrulation process, we have been using a transgenic line expressing a Histone H2A-RFP fluorescent protein, which allows us to visualize the movement of nuclei in developing embryos (Fig. 2b). Our time-lapse movie data is in the form of images, or more specifically, vectors of pixel intensities (Fig. 4a). Clearly, using all the pixel intensities as independent variables is excessive. In our method, we transform a pixelated image into a smaller set of independent variables which still capture the relevant features. We use principal component analysis (PCA) to reduce the original set of pixel vectors into a smaller set of independent variables [15, 16]. Generally, PCA projects data onto a linear subspace which captures the maximum variance in a data set (Fig. 4c). Often, a linear subspace of much lower dimension can capture most of the variance in the original high-dimensional data.

PCA yields a set of principal components or, in the context of images, *eigenimages* [17]. The eigenimages are ordered by the variance that they capture, such that the first image captures the greatest amount of variance in the data set (Fig. 5a). Often, we only need the first few eigenimages to describe most of the variability within the data set. Each of the images can now be described by a few coefficients which are the image's projection onto the eigenimages, rather than by the entire set of pixel intensities, thereby dramatically reducing the number of variables without a major loss of information (Fig. 4c) (*see* Note 8).

We can then consider fitting time as a function of these projection coefficients. We opt to use a simple linear functional form for the model, because it is both easy to fit and has explicit formulas for error bounds on the estimated response (Fig. 5c) [18, 19]. We assume that, given enough projection coefficients (independent variables), a linear model will be able to accurately predict the developmental time of an embryo snapshot.

Fitting a linear model to estimate the times of fixed images:

1. Begin with a set of n training images $I_1, \ldots, I_n \in \mathbb{R}^d$ (where each of the n images is a vector of d pixels) with associated times $t_1 \ldots, tn$ (Fig. 4a).
2. Preprocess the images as necessary: images should be in a consistent frame of reference, and the absolute pixel intensities should be meaningful for PCA. For

8. The PCA eigenimages cannot capture very fine-scale structures such as membranes, as these structures are not robust to noise in pixel-space.

Author Manuscript Author Manuscript Author Manuscript Author Manuscript

our data set, each image is resized to 100 × 100 pixels and rotated so that the ventral sides are at the bottom of the frame. To reduce inter-embryo noise, we symmetrize the image along the DV axis, by taking the average of the original image with its DV reflection. To account for intra-embryo variability, we normalize the intensity of each image, using adaptive histogram reweighting in the MATLAB image processing toolbox. Normalizing the nuclei channel intensity is permissible because the absolute intensity of the nuclei signal does not carry biological significance (*see* Note 9).

3. Compute the average image:

$$I_{\text{avg}} = \frac{1}{n}\sum_{j=1}^{n} I_j.$$

4. Construct the mean-centered data matrix (Fig. 4a):

$$Y = \begin{bmatrix} I_1 - I_{\text{avg}} \\ \vdots \\ I_n - I_{\text{avg}} \end{bmatrix} \in \mathbb{R}^{n \times d}.$$

5. Compute the right singular vectors E_1, …, En (assuming $n< d)$ of Υ, ordered in descending magnitudes of the corresponding singular values. These right singular vectors are the principal components/eigenimages (Figs. 4b and 5a).

6. Compute the projection coefficients $x_{ij} = I_i - I_{avg}, E_j$ for $i = 1,\ldots,n$ and $j = 1,\ldots,k$, where k is the number of retained projection coefficients (Fig. 5b). The procedure for choosing k will be discussed later.

7. Construct the matrix of projection coefficients:

$$X = \begin{bmatrix} 1 & x_{11} & x_{12} & \cdots & x_{1k} \\ 1 & x_{21} & x_{22} & \cdots & x_{2k} \\ \vdots & \vdots & \vdots & \ddots & \vdots \\ 1 & x_{n1} & x_{n2} & \cdots & x_{nk} \end{bmatrix} \in \mathbb{R}^{n \times k+1},$$

and the vector of associated times:

$$T = \begin{bmatrix} t_1 \\ t_2 \\ \vdots \\ t_n \end{bmatrix} \in \mathbb{R}^n.$$

8. Calculate the optimal regression coefficients for the linear model as

9. Image preprocessing is essential for estimating the time of gastrulating images, as this removes any variations due to staining and imaging.

Author Manuscript Author Manuscript Author Manuscript Author Manuscript

$$\begin{bmatrix}\beta_0\\ \beta_1\\ \vdots\\ \beta_k\end{bmatrix} = \left(X^T X\right)^{-1} X^T T,$$

the relative errors in the predicted times for each image:

$$\int_i = t_i - \left(\beta_0 + \beta_1 x_{i1} + \beta_2 x_{i2} + \ldots + \beta_k x_{ik}\right),$$

and the average error in the predicted times (Fig. 5c):

$$\sigma^2 = \frac{1}{n-k-1}\sum_{i=1}^{n}\int_i^2 .$$

9. To estimate the time of a new fixed image *I*., first preprocess the image as described in **step 2**. Compute the vector of projection coefficients:

$$x_* = \begin{bmatrix}1 & I_* - I_{\text{avg}}, E_1 & I_* - I_{\text{avg}}, E_2 & \cdots & I_* - I_{\text{avg}}, E_k\end{bmatrix},$$

and then calculate (*see* Note 10):

$$\xi_*{}^2 = \sigma^2 x_* \left(X^T X\right)^{-1} x_*^T .$$

10. The estimated time of the image I∗ is given by

$$t_* = \beta_0 + \beta_1 x_{*1} + \beta_2 x_{*2} + \ldots + \beta_k x_{*k} .$$

Assuming the regression errors are normally distributed, standard deviation error bars are given by $\pm\xi_*$.

The parameter *k* is chosen using cross-validation: the training data is divided into subsets or *folds,* and for each of these folds the selected data is removed and the remaining data is used to train a model. This model is used to predict the times for the removed data, and the errors in the predicted times *ei* are computed for this data. The parameter *k* is chosen where there is a plateau in the average error (Fig. 6a–c).

Procedure for choosing *k:*

1. For *k* = 1, 2, …:

a. Divide the data into folds (Fig. 6a).

10. DAPI can also stain “yolk nuclei” that have not reached the cortex and remain in the center of the embryo. These yolk signals need to be manually removed, since they can obscure PCA.

Author Manuscript Author Manuscript Author Manuscript Author Manuscript

b. For each fold.

- Define the remaining data (the data not in the selected fold) as the training data.
- Fit a model as described above.
- Using this model, calculate the errors *ei* in the predicted times for the held-out fold data (Fig. 6b).

2. Plot the root-mean-squared error as a function of *k;* choose *k* where this error plateaus (for our data, we take $k = 5$; *see* Fig. 6c).

Once *k* is chosen, the final model is fit using all the data.

Our training data consists of seven time-lapse movies spanning gastrulation, with images taken at 30-s intervals (*see* Note 7). When choosing *k,* each fold consists of the data from a single movie. From the principal components and regression function, we can estimate the age of a gastrulating embryo with precision of ~3 min.

3.4 Reconstruction of the Developmental Dynamics

With the developed membrane and PCA/regression time estimation protocols, we can estimate the developmental age of each of our fixed snapshots (Fig. 7a). We applied this protocol to a data set of embryos stained for dpERK and *ind* mRNA to reconstruct the developmental dynamics of ERK activation and the expression of this target gene. Once the snapshots are ordered in time, spatial patterns of dpERK and *ind* profiles can be extracted from raw confocal images. For example, we can extract the signal from a cell where *ind* is expressed and plot the change in signal intensity as a function of time, as shown in Fig. 7b, c. Embryo age *(x)* and signal intensity *(y)* are averaged over 5-min intervals to reduce interembryo variability. The reconstruction shows that ERK is activated as a pulse, where the signal increases superlinearly and decays exponentially (Fig. 7b). *ind* is expressed soon after ERK is activated and the expression level is maintained even after the decay of ERK activation (Fig. 7c).

Acknowledgements

B.L. and S.Y.S. were supported by the National Institutes of Health Grant R01GM086537. C.J.D. was supported by the Department of Energy Computational Science Graduate Fellowship (CSGF), grant number DE-FG02–97ER25308, and the National Science Foundation Graduate Research Fellowship, Grant No. DGE 1148900. I.G.K. was supported by the National Science Foundation (CDS&E program through CBET and CMMI).

References

1. Futran AS, Link AJ, Seger R et al. (2013) ERK as a model for systems biology of enzyme kinetics in cells. Curr Biol 23:R972–R979 [PubMed: 24200329]
2. Rauen KA (2013) The RASopathies. Annu Rev Genomics Hum Genet 14:355–369 [PubMed: 23875798]
3. Newbern J, Zhong J, Wickramasinghe RS et al. (2008) Mouse and human phenotypes indicate a critical conserved role for ERK2 signaling in neural crest development. Proc Natl Acad Sci U S A 105:17115–17120 [PubMed: 18952847]

Author Manuscript Author Manuscript Author Manuscript Author Manuscript

4. Dsilva CJ, Lim B, Lu H et al. (2015) Temporal ordering and registration of images in studies of developmental dynamics. Development 142:1717–1724 [PubMed: 25834019]
5. Lim B, Dsilva CJ, Levario TJ et al. (2015) Dynamics of inductive ERK signaling in the *Drosophila* embryo. Curr Biol 25:1784–1790 [PubMed: 26096970]
6. Gabay L, Seger R, Shilo BZ (1997) In situ activation pattern of *Drosophila* EGF receptor pathway during development. Science 277:1103–1106 [PubMed: 9262480]
7. Bronner G, Jackle H (1991) Control and function of terminal gap gene activity in the posterior pole region of the *Drosophila* embryo. Mech Dev 35:205–211 [PubMed: 1768621]
8. von Ohlen T, Doe CQ (2000) Convergence of dorsal, dpp, and egfr signaling pathways subdivides the *Drosophila* neuroectoderm into three dorsal-ventral columns. Dev Biol 224:362–372 [PubMed: 10926773]
9. Schneider CA, Rasband WS, Eliceiri KW (2012) NIH Image to ImageJ: 25 years of image analysis. Nat Methods 9:671–675 [PubMed: 22930834]
10. Kosman D, Mizutani CM, Lemons D et al. (2004) Multiplex detection of RNA expression in *Drosophila* embryos. Science 305:846 [PubMed: 15297669]
11. Coppey M, Boettiger AN, Berezhkovskii AM et al. (2008) Nuclear trapping shapes the terminal gradient in the *Drosophila* embryo. Curr Biol 18:915–919 [PubMed: 18571412]
12. Levario TJ, Zhan M, Lim B et al. (2013) Microfluidic trap array for massively parallel imaging of *Drosophila* embryos. Nat Protoc 8:721–736 [PubMed: 23493069]
13. Lecuit T, Samanta R, Wieschaus E (2002) slam encodes a developmental regulator of polarized membrane growth during cleavage of the *Drosophila* embryo. Dev Cell 2:425–436 [PubMed: 11970893]
14. Figard L, Xu H, Garcia HG et al. (2013) The plasma membrane flattens out to fuel cell surface growth during *Drosophila* cellularization. Dev Cell 27:648–655 [PubMed: 24316147]
15. Shlens J (2005) A tutorial on principal component analysis Systems Neurobiology Laboratory, University of California at San Diego, San Diego, CA
16. Jolliffe IT (2002) Principal component analysis Springer series in statistics, 2nd edn. Springer, New York, NY
17. Turk MA, Pentland AP (1991) Face recognition using eigenfaces. IEEE Comput Soc Conf Comput Vision Pattern Recogn 1991: 586–591
18. Wasserman L (2004) All of statistics : a concise course in statistical inference Springer texts in statistics. Springer, New York, NY
19. Heiberger RM, Holland B (2004) Statistical analysis and data display: an intermediate course with examples in S-plus, R, and SAS. Springer texts in statistics Springer, New York, NY
20. Chung K, Kim Y, Kanodia JS et al. (2011) A microfluidic array for large-scale ordering and orientation of embryos. Nat Methods 8:171–176 [PubMed: 21186361]

Author Manuscript Author Manuscript Author Manuscript Author Manuscript

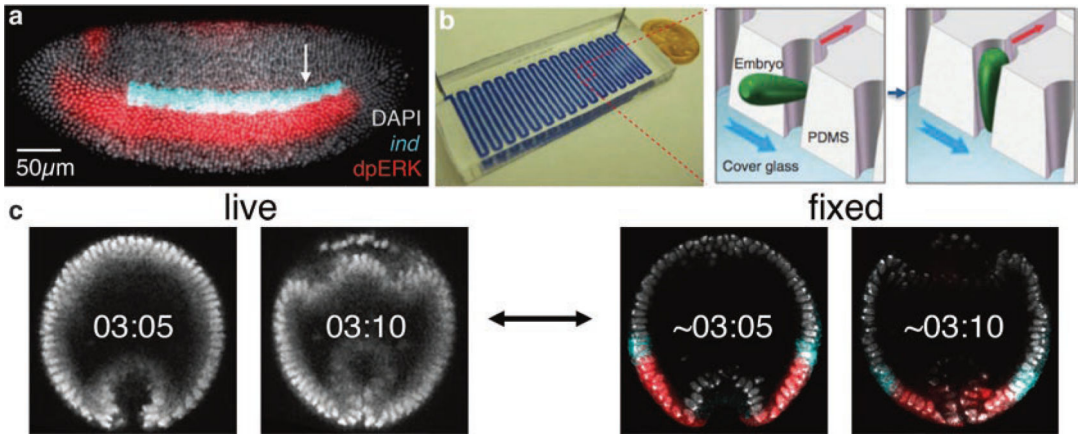

Fig. 1.

Quantitative analysis of the dynamics of ERK-dependent inductive signaling in the *Drosophila* embryo. (**a**) ERK activation (*red*) and expression of its target gene *ind (cyan)* in the early embryo. The *arrow* indicates the position at which DV cross-sections are imaged in the microfluidic device. (**b**) Microfluidic device used to vertically orient embryos, and schematics of embryo trapping in vertical orientation [figures adapted from [20]]. (**c**) Snapshots of live Histone 2A-RFP (His-RFP) embryos *(left),* which are used as a wild-type strain to visualize nuclei, and fixed embryos stained with DAPI *(gray),* dpERK antibody *(red),* and *ind* mRNA probe *(cyan) (right).* The developmental age of fixed embryos can be estimated by matching the morphology between live and fixed embryos. DAPI (1:10,000) was used to stain for nuclei. Monoclonal rabbit anti-dpERK (1:100; Cell Signaling) and sheep anti-digoxygenin (1:125; Roche) antibodies were used to visualize ERK activation and *ind* expression pattern

Author Manuscript Author Manuscript Author Manuscript Author Manuscript

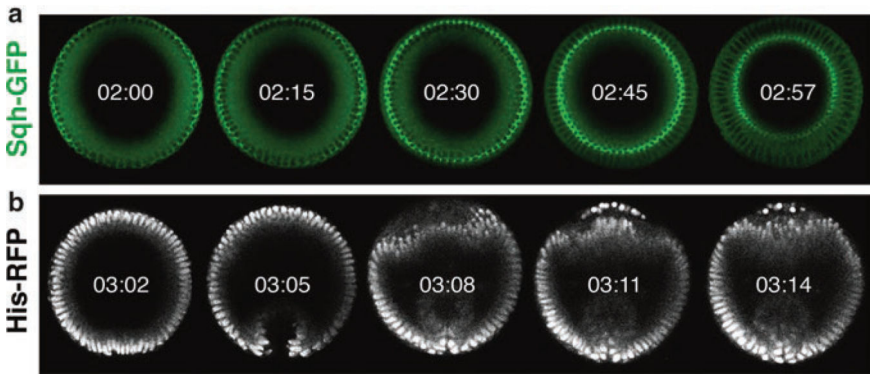

Fig. 2.

Live imaging of cellularization and gastrulation. (**a**) Selected frames from live imaging of Sqh-GFP embryos during cellularization. (**b**) Selected frames from live imaging of His-RFP embryos during gastrulation. *Times* indicate the developmental ages (hours after egg-laying) of embryos

Author Manuscript Author Manuscript Author Manuscript Author Manuscript

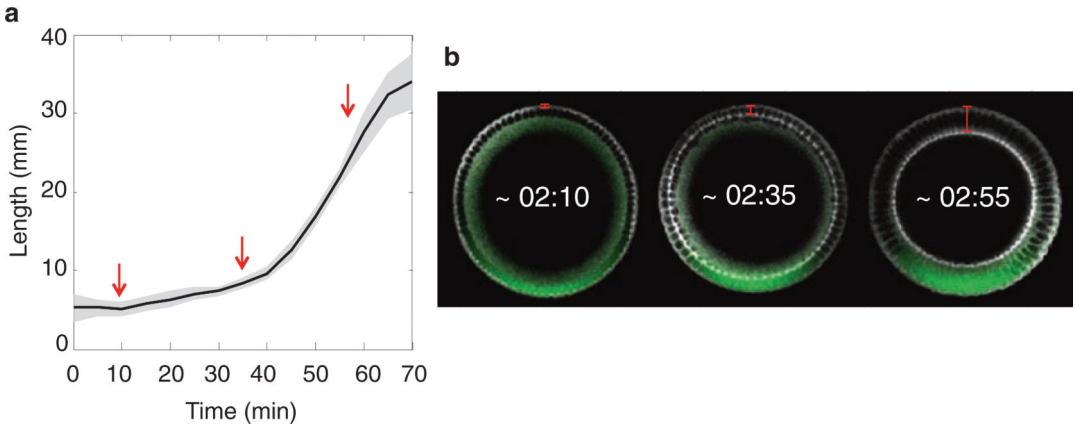

Fig. 3.

Estimating the developmental time of fixed embryos during cellularization. (**a**) Calibration curve relating invaginating membrane length and developmental time generated from six time-lapse recordings of Sqh-GFP expression; *time* indicates minutes after 2 h from egg-laying. *Red arrows* indicate the points corresponding to the images in (**b**). The standard deviation of the six movies is shown in *gray.* (**b**) Fixed embryos stained for Myosin II HC *(gray)* and Dorsal *(green). Red segments* indicate the increasing furrow lengths of selected embryos. Estimated times inferred from the calibration curve are indicated for each image. Rabbit anti-Myosin II HC/Zipper (1:100; gift from Eric Wieschaus, Princeton University), and mouse anti-Dorsal (1:100; Developmental Studies Hybridoma Bank) antibodies were used

Author Manuscript Author Manuscript Author Manuscript Author Manuscript

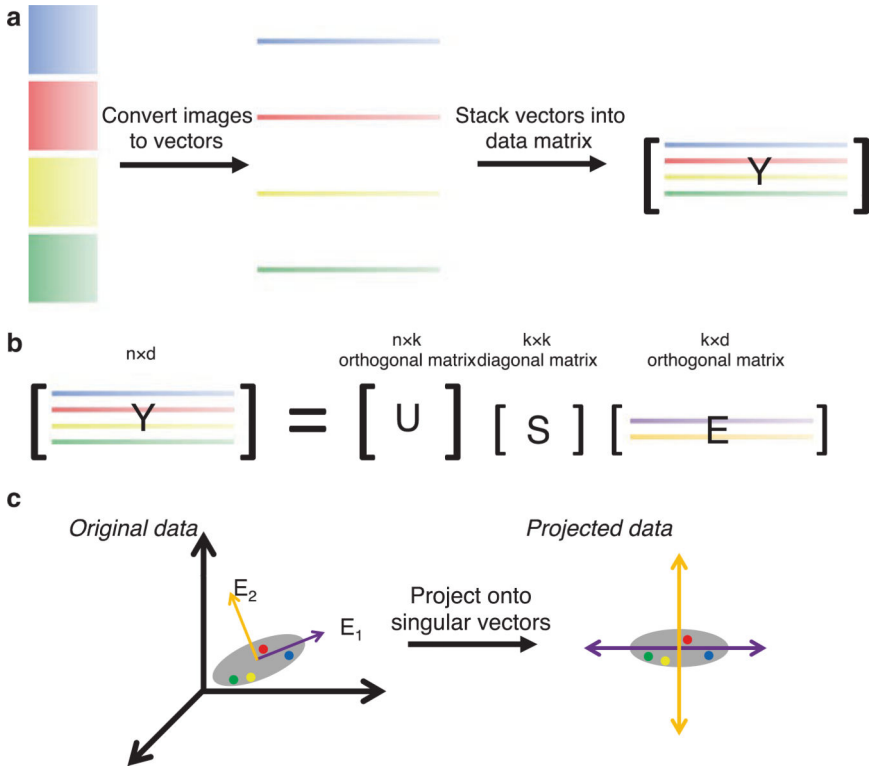

Fig. 4.

Using PCA to reduce image dimension. (**a**) Schematic illustrating the conversion of images to a data matrix. The mean-centered images are first converted to vectors by unwrapping the two-dimensional array of *d* pixel intensities into one-dimensional *d*-long vectors. The vectors are then stacked into a data matrix *Y.* (**b**) Illustration of computing the principal components of a data set. The data matrix *Y* is factored using singular value decomposition (SVD) into the product of an orthogonal matrix *U,* a diagonal matrix *S*, and an orthogonal matrix E, where the entries of the diagonal matrix *S* are in non-increasing order. The rows of *E* contain the principal components or eigenimages of the data. (**c**) Illustration of projecting the data onto the first few principal components. The d-dimensional data are projected onto the first few right singular vectors (*E*) of the matrix *Y,* where the projection coefficients are given by the entries of the matrix *U.S.* If the entries of *S* (the singular values) decay rapidly, then the first few singular vectors capture most of the information contained in matrix *Y.* Each data point (each image) can be described using the first few projection coefficients, rather than the entire vector of pixel intensities

Author Manuscript Author Manuscript Author Manuscript Author Manuscript

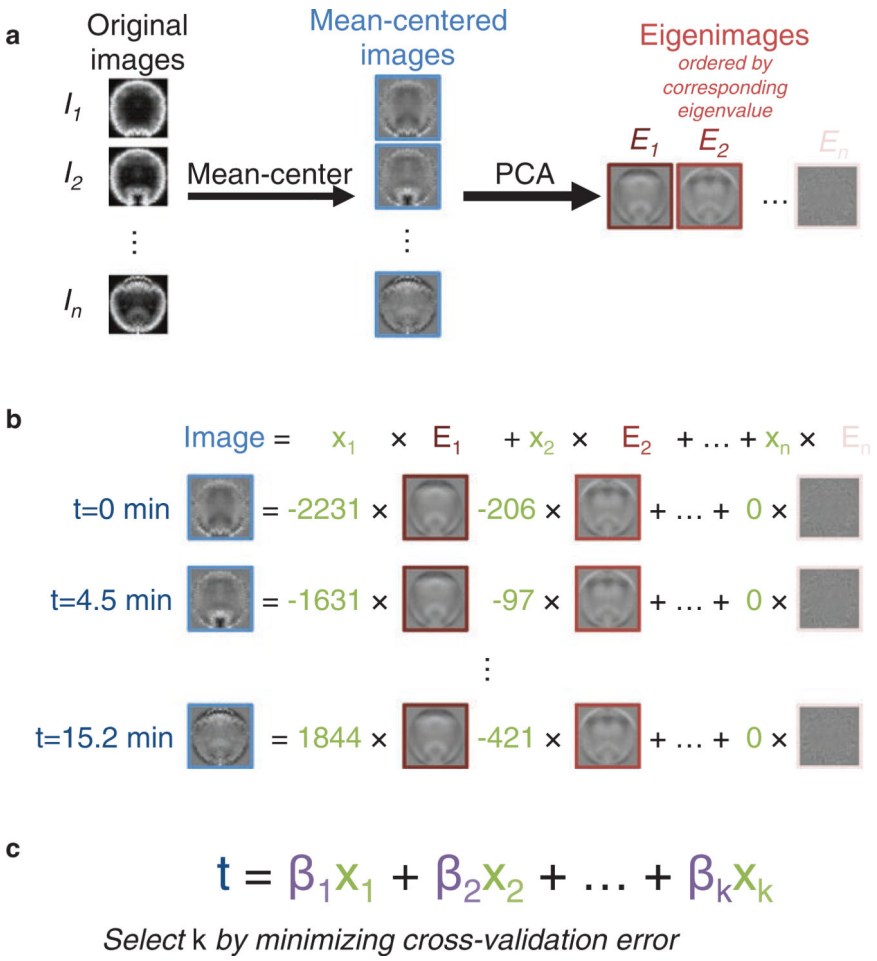

Fig. 5.

Fitting a linear model to estimate the times of fixed images. (**a**) Illustration of PCA on the imaging data set. The training images obtained from live imaging of *Drosophila* embryos during gastrulation are first mean-centered. The eigenimages for this data are then obtained by computing the singular vectors of the data matrix. (**b**) Illustration of decomposing the images using their projection coefficients. For each image in the live imaging data set, the projection coefficients onto the eigenimages are calculated. Each image is then the weighted sum of eigenimages, with weights given by the projection coefficients. (**c**) A linear model for time as a function of the first *k* projection coefficients is fit using the live imaging data as training data

Author Manuscript Author Manuscript Author Manuscript Author Manuscript

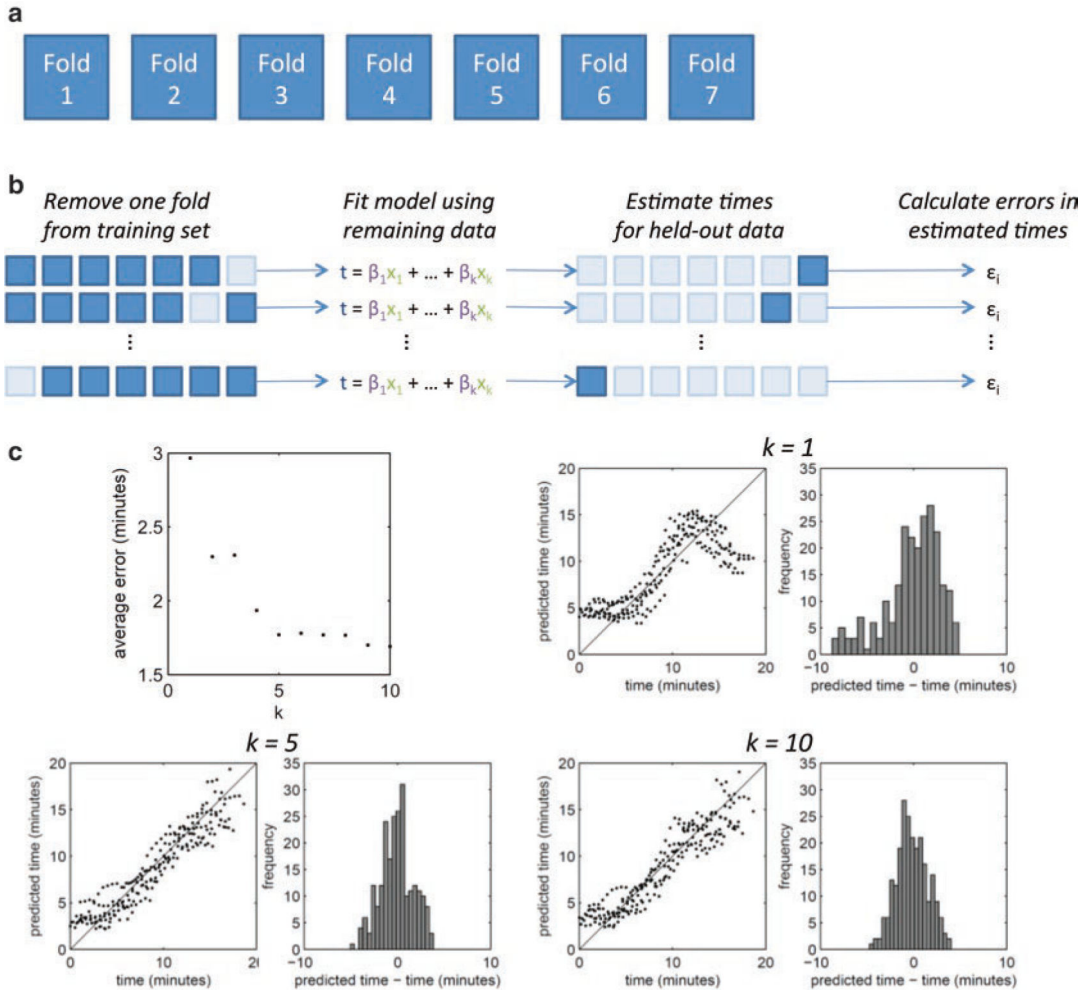

Fig. 6.

Choosing the number of retained projection coefficients *k*. (**a**) Schematic depicting the data divided into folds. In our case, each fold consists of the images from an independent live imaging experiment. (**b**) Illustration of the cross-validation procedure. For each of the folds, the data from that given fold is removed from the training data. The remaining live imaging data (six movies in this example) is used to train a linear model of time as a function of the first *k* projection coefficients (as described previously). This model is used to predict the times for the left-out fold data, and the errors in the estimated times are computed. (**c**) The root-mean-squared error (RMSE) in the predicted times are plotted as a function of *k* (the number of projection coefficients used in the linear model). The parameter *k* is chosen where there is a plateau in the RMSE (in this case, we choose $k = 5$). The predicted versus true times, as well as the distribution of errors in the predicted times, are shown for several values of *k*

Author Manuscript Author Manuscript Author Manuscript Author Manuscript

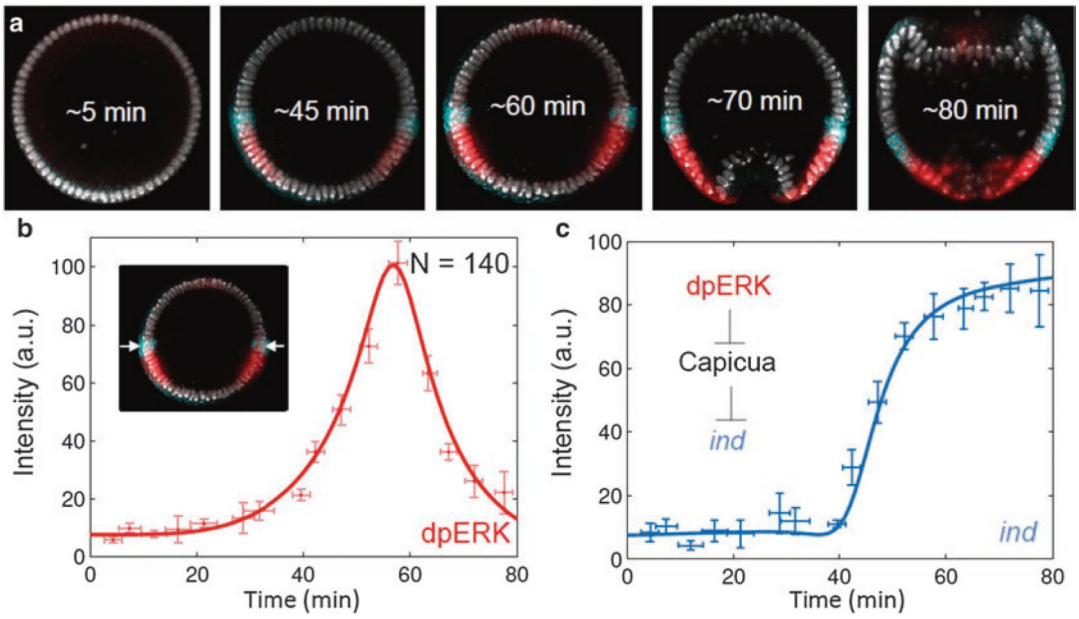

Fig. 7.

Reconstruction of ERK activation and expression of *ind.* (**a**) Dorsoventral cross-sectional images of embryos costained with DAPI (*gray*), dpERK antibody *(red),* and *ind* mRNA probe *(cyan).* Estimated developmental age of each fixed embryo is indicated (0 min is defined as the onset of nuclear cycle 14, which takes place approximately 2 h after egg-laying). (**b**, **c**) Reconstruction of ERK activation and *ind* expression kinetics during the third and fourth hours of development. The *arrow* in the *inset* of (**b**) indicates the position of *ind* expression where the signal is extracted to plot the time course. In this domain, ERK is activated as a pulse whereas *ind* is expressed in a step-like manner from minutes 40 onwards. Figure is adapted from [5]